Crystallization kinetics of Al2O3-26mol%Y2O3 glass and full crystallized transparent Y3Al5O12-based nanoceramic

Ying Zhang, Xiaoguang Ma, Xiaoyu Li, Lixia Yang, Binghui Ge, Mathieu Allix, Jianqiang Li

Crystallization kinetics of Al_2O_3-26mol%Y_2O_3 glass and full crystallized transparent $Y_3Al_5O_{12}$-based nanoceramic

Ying Zhang [a,b], Xiaoguang Ma [a], Xiaoyu Li [a,b], Lixia Yang [c], Binghui Ge [d,e,**], Mathieu Allix [f], Jianqiang Li [a,b,*]

[a] National Engineering Laboratory for Hydrometallurgical Cleaner Production Technology, CAS Key Laboratory of Green Process and Engineering, Institute of Process Engineering, Chinese Academy of Sciences, Beijing, 100190, China
[b] University of Chinese Academy of Sciences, Beijing, 100049, China
[c] Beijing National Laboratory for Condensed Matter Physics, Institute of Physics, Chinese Academy of Sciences, Beijing, 100190, China
[d] Institutes of Physical Science and Information Technology, Anhui University, Hefei, 230601, China
[e] Key Laboratory of Structure and Functional Regulation of Hybrid Materials (Anhui University), Ministry of Education, Hefei, 230601, China
[f] CNRS, CEMHTI UPR 3079, Univ. Orléans, 45071, Orléans, France

ARTICLE INFO

Keywords:
Transparent YAG-Al_2O_3 ceramics
Nanoceramics
YAG glass
Crystallization kinetics

ABSTRACT

Transparent $Y_3Al_5O_{12}$-based polycrystalline ceramics with excessive Al_2O_3 composition (Al_2O_3-26 mol%Y_2O_3, AY26) have been demonstrated as potential host materials for phosphor applications. However, the crystallization mechanism of AY26 glass has not been thoroughly investigated so far. In this work, the non-isothermal crystallization kinetics of AY26 glass was experimentally analyzed. The AY26 glass depicts high activation energy and crystallization mechanism of volume nucleation followed by three-dimensional crystal growth mode. Based on the analysis, a novel highly transparent YAG-Al_2O_3 nanoceramic material was elaborated at lower temperature of 963 °C by using pressureless glass crystallization. The biphase nanoceramic is characterized by the structure of YAG nanocrystals surrounded with homogeneous thin Al_2O_3 layers. It is extremely transparent from visible to mid-infrared region, particularly the transmittance can reach the theoretical limit of YAG transparent ceramic in NIR and MIR regions. Besides, it has almost same hardness of 21 GPa with YAG single crystal and YAG transparent ceramic.

1. Introduction

Yttrium aluminum garnet $Y_3Al_5O_{12}$ (YAG) transparent ceramics have become a competitive substitute of YAG single crystals as host materials for solid state lasers, phosphors, and scintillators due to the advantages of the elaboration process (time-saving production period, low cost) and product characteristics (geometric versatility, relatively swift scalable manufacturing, and doping flexibility) [1–6]. In the last decades, various sintering synthetic approaches have been employed to synthesize the YAG transparent ceramics, such as spark plasma sintering [7,8], vacuum sintering [9], and hot isostatic pressing sintering [10]. To perform the sintering processes, high quality nanoscale raw powders (e.g. high purity, free of aggregation), high-pressure and high-sintering temperature are indispensable for eliminating light scattering sites such as residual pores and secondary phases in the ceramic bulks. On the other hand, nanosized grains in transparent ceramics have been desired since the light Rayleigh scattering is largely weakened, as well as the mechanical properties of transparent ceramics are also significantly enhanced by Hall-Petch effect in comparison to micro-grainsized transparent ceramics [2,11]. By using usual sintering techniques, however, elaboration of highly transparent ceramics with nanocrystalline is still a challenge due to rapid grain growth at high sintering temperature [11]. For instance, as-sintered Dy:YAG ceramics at 1780 °C for 8 h under 10^{-3} Pa vacuum condition were always found with ubiquitous tens micrometer grains even using ultrafine raw powders of Al_2O_3 (200 nm) and Y_2O_3, Dy_2O_3 (80 nm) [12].

Full crystallization from melt-solidified glass has been recognized as a promising approach to synthesize fully dense polycrystalline ceramics.

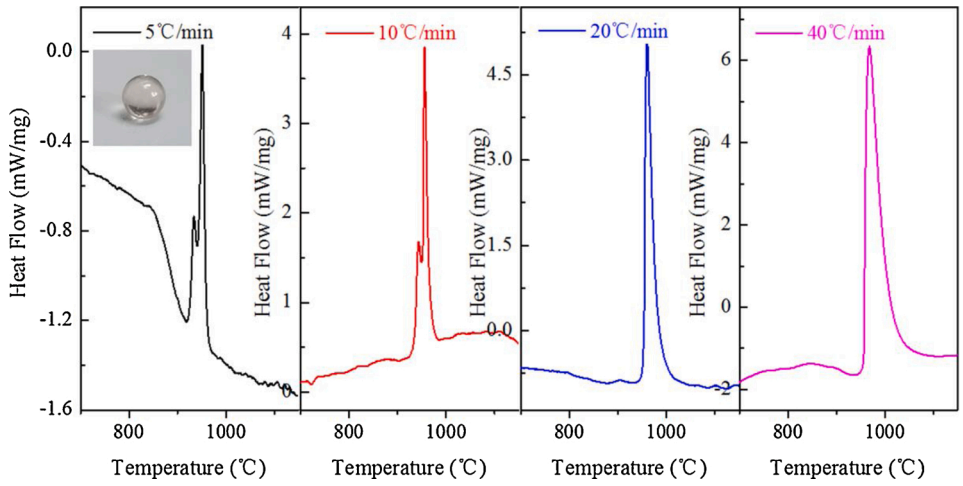

Fig. 1. DSC curves of unbroken AY26 glass beads (2.5 mm) at different heating rates of 5, 10, 20, and 40 ℃·min^{-1}. Transparent glass bead with a diameter of 2.5 mm synthesized using aerodynamic levitation coupled to a laser heating system is embedded.

M. Allix et al. have successfully fabricated a series of fully crystallized transparent ceramics with micrometer-sized structure [13–20], including aluminate ($Sr_3Al_2O_6$ [13], $BaAl_4O_7$ [14], (100-z)$BaAl_4O_7$-z$BaAl_2O_4$ ($0 < z \leq 45$) [15]), silico-aluminate ($Sr_{1+x/2}Al_{2+x}Si_{2-x}O_8$ ($0 < x \leq 0.4$) [16], $Sr_{1-x/2}Al_{2-x}Si_xO_4$ ($0.2 \leq x \leq 0.5$) [17]), etc, through the simply pressureless glass crystallization route. By comparison, highly transparent ceramics with nanocrystalline synthesized using full crystallization from bulk glasses required harsh process, such as the ultrahigh external pressure for silicate garnet [11], whereas there is only 55 % transmittance at 800 nm (1 mm thick) for transparent LaAlO$_3$/t-ZrO_2 (53 %Al_2O_3-20 %La_2O_3-27 %m-ZrO_2) nanoceramic crystalized from bulk glass under a moderate process [21]. Up to now, transparent YAG ceramics with nano-sized structure has been rarely reported, much less by full crystallization approach. In our recently previous work, the 74 mol%Al_2O_3-26 mol%Y_2O_3 (AY26) bulk glass using containerless solidification process was fully crystallized (at 1100 □) into a YAG-based transparent nanoceramic, thus showing that presurelessly full crystallization from glass can be a successful synthetic route to densify YAG-based transparent ceramics with nanostructures [22].

The knowledge on crystallization mechanism is essential for controlling glass crystallization into transparent ceramics. The crystallization mechanism of stoichiometric $Y_3Al_5O_{12}$ glass has been deeply investigated in the last few decades, but opaque polycrystalline ceramics with submicron and micron YAG crystals have been usually obtained [23–26]. For instance, as reported by A. Prnová et al. the apparent activation energy of glass microspheres with stoichiometric YAG composition was 1100 ± 10 kJ mol^{-1} and a three-dimensional crystal growth was determined [25]. The presence of regularly spaced YAG crystals with size ≤ 1 μm was observed in the whole volume of fully crystalline microspheres. To date, there is no report on the crystallization mechanism of the AY26 bulk glass. Non-isothermal thermal analysis is regarded as a very useful tool for studying the crystallization kinetics of glasses as it is a rapid and convenient mean [27–30]. In this work, the crystallization behavior of the AY26 glass was experimentally investigated and theoretically analyzed using Kissinger, Augis-Bennett, and Ozawa models. Afterwards, YAG-Al_2O_3 nanoceramics were prepared by full crystallization from the AY26 glass heat treated at 963℃. The microstructure and optical property of the YAG-Al_2O_3 nanoceramic were examined and discussed.

2. Experimental procedure

2.1. Preparation of AY26 glass and YAG-Al_2O_3 transparent ceramic

Commercial oxide powders Al_2O_3, Y_2O_3 (Sinopharm chemical reagent co. ltd) with 99.99 % purity were used as starting materials. The powders were weighed according to the composition of 74 mol% Al_2O_3-26 mol% Y_2O_3 (3.02 g Al_2O_3, 2.35 g Y_2O_3), and homogeneously mixed by wet ball milling using ethanol. After being dried at 50 ℃ in an air drying oven for 2 h, the powders were pressed into pellets and then placed in an aerodynamic levitation coupled to a laser heating system. The pellet was suspended using oxygen with ≥99.99 % purity, and heated to 2100 ℃ and held for a few seconds, and subsequently quenched down to room temperature at roughly 250 ℃·s^{-1} by shutting off ; the CO_2 lasers. Transparent glass beads with diameters of ~2−5 mm were prepared and subsequently polished into disks. These disks were heated to 963 ℃, and held separately for different periods of time in an open-air atmosphere muffle furnace to prepare transparent ceramics.

2.2. Characterization

The phase crystallinity and nature of the samples were identified by X-ray powder diffraction (SmartLab-9, Rigaku Corp.) with Cu Kα radiation. The nanostructures were observed by transmission electron microscope (TEM, JEM ARM200 F). Thermal behaviors of the AY26 glass beads and powders were measured using differential scanning calorimeter (DSC, Setaram MULTI HTC 1600 instrument) using argon as the purging gas and with alumina pans as sample holders. The optical transmittance of the samples was recorded using a UV–Vis-NIR spectrophotometer (PERSEE TU-1901, Beijing, China) in the 190−2500 nm wavelength range, and a Fourier-transform infrared spectrometer (Shimadzu FTIR 8200, Kyoto, Japan) in the 2500−8000 nm range. The hardness and Young's modulus of the samples were measured with a nanoindenter (MTS-XP), and the force and displacement were 600 mN and 1400 nm, respectively. At least eight indentations were made on each sample using a Berkovich-type diamond indenter.

3. Results and discussion

3.1. Crystallization kinetics analysis of AY26 glass

A detailed crystallization kinetic analysis, providing information on the crystallization mechanism of a glass, involves the determination of the activation energy (E_a) of crystallization, Avrami parameter (n) and dimensionality (m) of crystal growth. The E_a value reflects the sensitivity

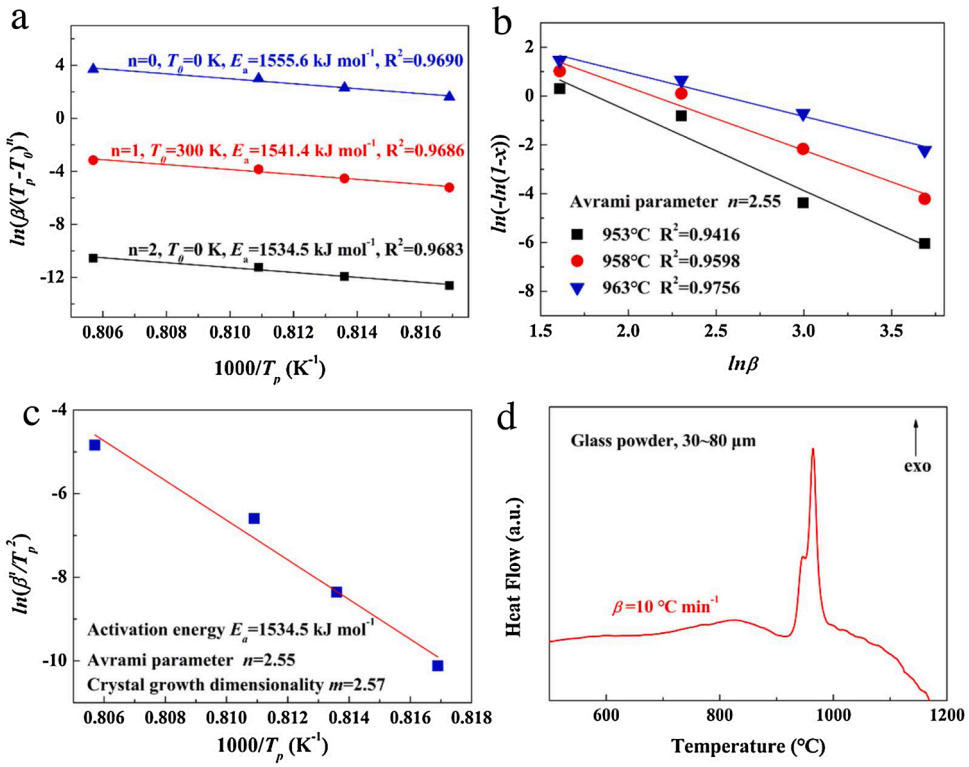

Fig. 2. (a) Plots of $\ln[f_{(\alpha)}(\beta/(T_p-T_0)^n)]$ vs $(1000/T_p)$, (b) plots of $ln[-ln[f_{(\alpha)}(1-x)]]$ vs $ln[f_{(\alpha)}\beta]$, and (c) plot of $ln[f_{(\alpha)}(\beta^n/T_p^2)]$ vs $(1000/T_p)$. (d) DSC curve of AY26 glass powder (30~80 μm) under constant heating rate of 10 ℃·min^{-1}.

of a glass to temperature variation and thus affects the controllability of a crystallization process, whereas n and m values reflect nature of the crystallization mechanism [31]. Batches of AY26 glass beads with identical diameter of 2.5 mm were used to perform non-isothermal experiments, one of which is embedded in Fig. 1. The DSC curves of these AY26 glass beads at different heating rates (β = 5, 10, 20, and 40 ℃·min^{-1}) were recorded for non-isothermal crystallization kinetics analysis. Fig. 1 show the large exothermic peaks on DSC curves with different heating rates which were corresponded to the crystallization of the YAG phase. The peak crystallization temperature T_p increases from 950 ℃ to 967 ℃ when the heating rate increases from 5 ℃· min^{-1} to 40 ℃· min^{-1}. The peak crystallization temperature and corresponding heating rate are used to estimate the crystallization activation energy E_a through established models such as Kissinger, Augis-Bennett, and Ozawa models [32, 33].

The Kissinger model considering the heating rate dependence of the peak crystallization temperature is widely applied to calculate E_a, as given in the following equation [34]:

$$\ln\left(\frac{\beta}{T_p^{\,2}}\right) = -\frac{E_a}{RT_p} + const$$

Where β is the heating rate, T_p is the peak crystallization temperature, and R is the gas constant. Another model based on approximation method proposed by Augis and Bennett is shown as the following equation [35]:

$$\ln\left(\frac{\beta}{T_p - T_0}\right) = -\frac{E_a}{RT_p} + lnK_o$$

Where T_0 is typically 300 K and K_0 is the frequency factor. Last, the Ozawa model considering the case that the degree of reaction is constant and independent of the heating rate is described by the following equation [36]:

$$\ln\beta = -\frac{E_a}{RT_p} + const$$

Fig. 2a represents the plots of $\ln(\beta/(T_p - T_0)^n)$ vs $(1000/T_p)$ in case of n = 2, 1, 0 for Kissinger, Augis-Bennett, and Ozawa models, respectively. T_0 is 0 K for Kissinger and Ozawa models, while T_0 is 300 K for Augis-Bennett model. The activation energies calculated from the slopes of the plots $\ln(\beta/(T_p - T_0)^n)$ vs $(1000/T_p)$ are 1535, 1541, and 1556 kJ·mol^{-1} for Kissinger, Augis-Bennett, and Ozawa models, respectively. The activation energy values of the AY26 glass obtained from these models are very close and much higher than that of previously reported stoichiometric YAG glasses (437 kJ· mol^{-1} reported by B. R. Johnson et al. [23]; 578 ± 16 kJ· mol^{-1} reported by G. He et al. [24]; 1100 ± 10 kJ· mol^{-1} reported by A. Prnová et al. [25].) This result indicates that an excess of Al_2O_3 in AY26 glass gives rise to its better thermal stability and higher sluggishness to crystallization than YAG glass.

The Avrami parameter (n) is considered to be related to crystallization mechanism, which could be determined according to the following equation [28]:

$$\left.\frac{dln[-\ln(1-x)]}{d\ln\beta}\right|_{T_y} = -n$$

Where x is the volume fraction of the crystalline phase at a given temperature T_y. The linear fitting of $ln[-ln(1-x)]$ vs $ln\beta$ is shown in Fig. 2b. The n obtained from the slope of the fitted straight line is 2.55. Besides, the Avrami parameter (n) is related to the dimensionality (m) of the crystal growth, and m can be calculated from the modified equation by Matussita and Sakka [37]:

$$\ln\left(\frac{\beta^n}{T_p^{\,2}}\right) = -\frac{mE_a}{RT_p} + const$$

Where the activation energy E_a is determined to be 1535 kJ· mol^{-1}

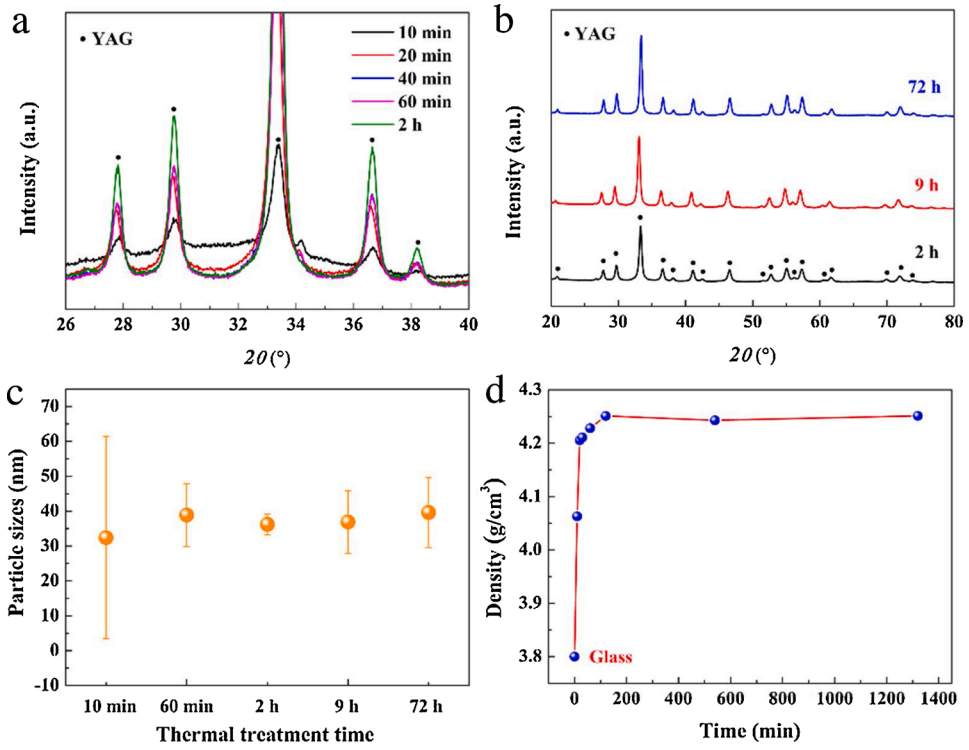

Fig. 3. (a) and (b) The XRPD patterns, (c) crystallite sizes, and (d) densities of AY26 glass and transparent samples crystallized from AY26 glasses at 963℃ for different durations.

according to the Kissinger model, and n is 2.55. The plot of $\ln(\beta^n/T_p^2)$ vs $(1000/T_p)$ is presented in Fig. 2c. Last, the crystallization dimensionality parameter $m = 2.57$ is obtained from the slope and appears very close to the Avrami parameter (n), signifying that the number of nuclei does not change with the heating rate [38], and that the crystallization mechanism of AY26 glass is volume nucleation followed with three-dimensional crystal growth. Moreover, several AY26 glass beads (2.5 mm of diameter) were ground into powders with particle size of 30~80 μm. As shown in Fig. 2d, the DSC curve of the glass powder at the heating rate of 10 ℃· min^{-1} shows a same variation trend with that of unbroken AY26 glass bead at the same heating rate, which further demonstrates the volume nucleation mechanism.

3.2. *Preparation of transparent YAG-Al_2O_3 nanoceramics*

In our previous work, transparent YAG-based nanoceramics were elaborated through crystallization of the AY26 glass using a heating rate of 10 ℃· min^{-1} and a dwell of 2 h at 1100 ℃ [22]. In order to explore a lower crystallization temperature and further compare the structure and properties of samples crystallized at different temperature, the AY26 glass beads were hold at 963 ℃, the temperature slightly above the crystallization peak, with the same heating rate of 10 ℃· min^{-1}. A series of bulk samples were heated at 963 ℃ for varied durations from 10 min to 72 h to investigate optimal process condition, and their X-ray powder diffraction (XRPD) patterns are presented in Fig. 3a. Diffraction peaks of YAG crystalline phase can already be observed in the XRPD pattern of sample crystallized for 10 min. And the intensity of YAG diffraction peaks increases gradually with the increasing of heat treatment duration, but the half-peak width remains basically unchanged. No other crystalline phases except the YAG crystalline phase arise in the sample even though the heat treatment time reaches 72 h (Fig. 3b), indicating that the AY26 glass possibly crystallized completely within 2 h. The crystallite sizes of samples crystallized for durations varying from 10 min~72 h were calculated by Scherrer's formula [39]:

$$D = \frac{K\gamma}{\beta cos\theta}$$

Where D is the crystallite size of the material, K is the Scherrer constant valued as 0.89, β is the half-height width of the diffraction peak of the samples measured, and the peak at 33.3°(2θ) is used to calculate the crystallite size, θ is the diffraction angle, γ is the X-ray wavelength of 0.154056 nm. Considering strain effect correction, the calculated crystallite sizes of samples crystallized for different durations are illustrated in Fig. 3c. Due to incomplete crystallization, there is a large deviation in the calculated crystallite size of the sample crystallized for 10 min. The calculated crystallite size of the ceramic crystallized at 963 ℃ for 2 h is ~36 nm, which is smaller than that of the reported YAG-based nanoceramic obtained at 1100℃ (51 ± 2 nm) in our reported work [22]. The growth of crystallite size is very limited, even if the heat holding time reaches 72 h, indicating that the transparent ceramics crystallized at 963 □ for 2 h show excellent thermal stability at the temperature of 963 ℃. Fig. 3d shows the variation curve of the sample density with the heat treatment time. The density of AY26 glass is 3.8 g· cm^{-3}, and it increased to 4.25 g· cm^{-3} when the heat treatment time extended to 2 h, signifying that a large volume shrinkage (11.8 %) occurred. When the heat treatment prolonged from 2 h to 22 h, density changed very limited, further confirming that the AY26 glass crystallization completed within 2 h.

Transmission electron microscope (TEM) micrographs of transparent ceramic crystallized at 963 ℃ for 2 h are given in Fig. 4. It can be clearly seen from Fig. 4a that the resulting transparent ceramic consists of nanocrystals. High-resolution transmission electron microscopy (HRTEM) micrograph and the related Fourier transformation diffractograms embedded in Fig. 4b clearly exhibit the presence of two strong crystalline phases of YAG phase and Al_2O_3 phase. Because of the difference in average atomic number (obtained from the sum of the atomic numbers (Z) of all atoms composing a phase divided by the number of atoms) between YAG ($Z_{YAG} = 14$) and Al_2O_3 ($Z_{Al2O3} = 10$), two different phases with strong contrast difference were observed by the method of high angle annular dark field-scanning transmission electron

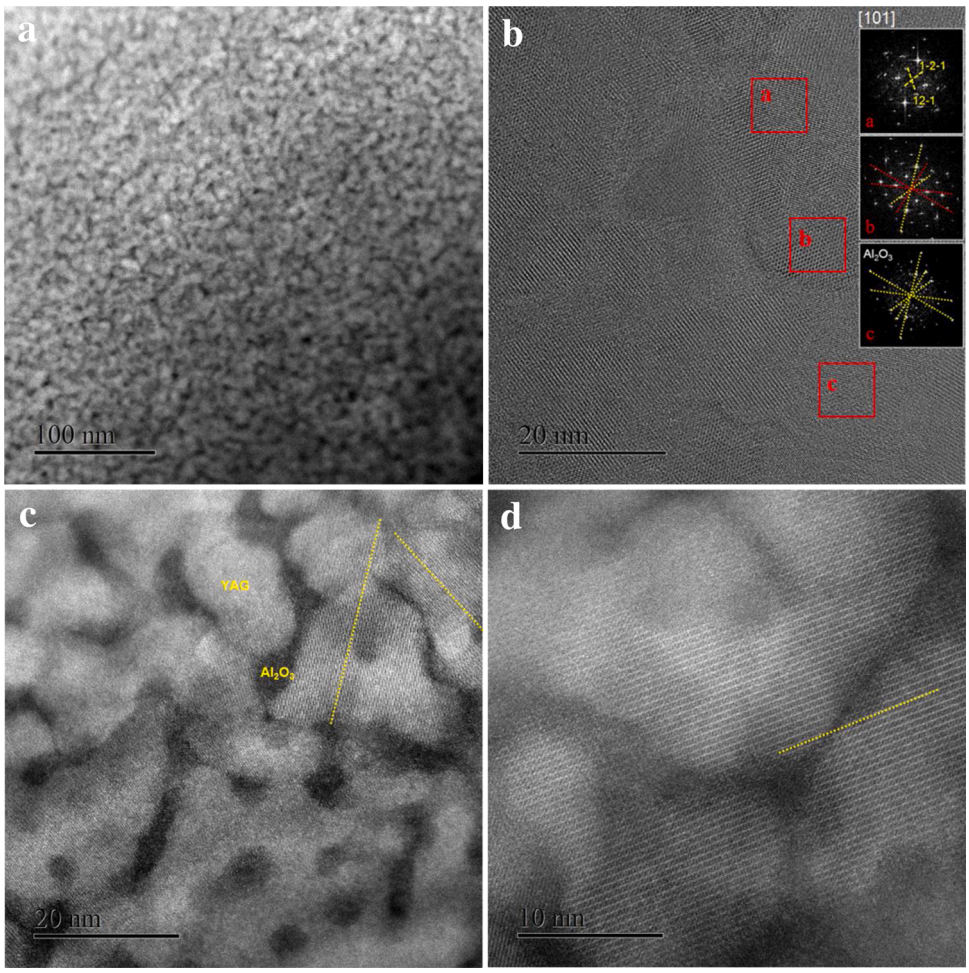

Fig. 4. TEM micrographs of transparent YAG-Al_2O_3 nanoceramic crystallized from AY26 glass at 963℃ for 2 h, and insets in (b) are the Fourier transformation diffractograms of the selected areas indicated by squares.

microscopy (HAADF-STEM), as shown in Fig. 4c and d. The bright phase is YAG phase, and the black phase around YAG phase is Al_2O_3 phase, both of which together form an interconnected composite nanostructure. Therefore, it is actually a YAG-Al_2O_3 composite ceramic crystallization from bulk AY26 glass. It is clear that the nanoceramic is a typical strong volume crystallization mechanism, which is consistent with the crystallization kinetics analysis. The as-prepared transparent ceramics remains fully dense like its glass precursor without any cracks and pores despite a large volume shrinkage (11.8 %) occurred by YAG crystallization. It is reasonable to infer that the shrinkage stress during YAG crystallization is effectively released by structural relaxation of the thin Al_2O_3 layers [22]. It is worthy to note that not only identical orientations but also distinct misfit between YAG grains crystallographic orientations exist in the transparent ceramic crystallized at 963 ℃ for 2 h. For the reported YAG-based nanoceramic crystallized at 1100 ℃, the misfit between YAG grains crystallographic orientations was very small, and a clear coalescence growth was demonstrated [22]. Furthermore, an in-situ HRTEM observation was also performed on the AY26 glass to monitor its crystallization process. It was found that a large amount of YAG nuclei firstly occurred from the glass and then Al_2O_3 layers formed from the residual Y_2O_3-lacked matrix. The whole process proceeded very rapidly and completed in seconds. The presence of thin Al_2O_3 barriers most probably has a positive effect in restraining YAG grain growth rate during crystallization process, implying that a self-limited growth mechanism must be taking place [40,41].

The transmittance spectra of a YAG-Al_2O_3 nanoceramic crystallized at 963 ℃ for 2 h, a YAG single crystal, and a stoichiometric YAG

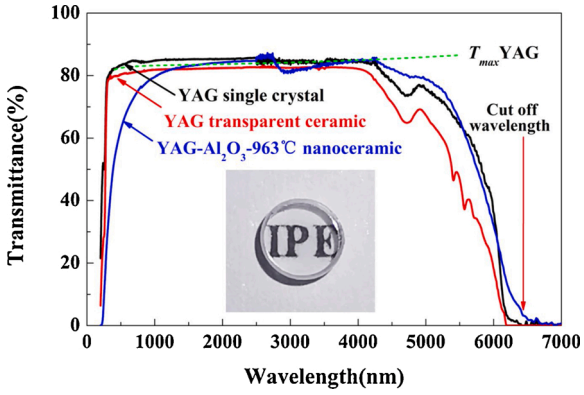

Fig. 5. Optical transmittance measured through 1.5 mm thick samples in UV–Vis-NIR and MIR region of the YAG-Al_2O_3 nanoceramic crystallized at 963 ℃ for 2 h, YAG single crystal, and micrometer scale YAG transparent ceramic. The photograph of the YAG-Al_2O_3 nanoceramic is embedded.

transparent ceramic (of 30 μm average crystallites size) were measured through 1.5 mm thick disks in UV–Vis-NIR and MIR regions, as shown in Fig. 5. A photograph of the YAG-Al_2O_3 nanoceramic is embedded. The dotted dark green line corresponds to the theoretical maximum transmittance of YAG transparent ceramics [42]. It can be seen that the transparent YAG-Al_2O_3 nanoceramic shows a high transparency in the visible to mid-infrared range, even the transmittance reaches the

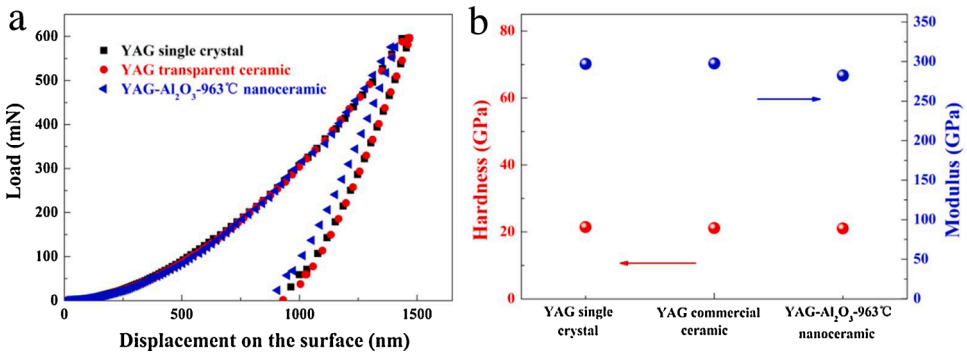

Fig. 6. (a) Typical load-displacement curves, and (b) hardness and Young's modulus of the YAG-Al_2O_3 nanoceramic crystallized at 963 ℃ for 2 h, YAG single crystal and micrometer scale YAG transparent ceramic.

theoretical maximum transmittance of YAG transparent ceramics in the NIR and MIR regions (1500−4300 nm). The absorption band located around 3 μm is attributed to the absorption of free hydroxyl (OH) group [22]. Compared with the YAG-based nanoceramic crystallized at 1100 □ [22], the nanoceramic crystallized at 963 ℃ for 2 h demonstrates higher transmittance over the whole studied window, which may be attributed to reduced light scattering linked to smaller grain sizes according to the Rayleigh-Gans-Debye theory. In addition, the resulting YAG-Al_2O_3 nanoceramic has a lower transmittance in the visible light region than YAG single crystal and the stoichiometric YAG transparent ceramic due to the light scattering caused by the refractive index difference between the small amount of the Al_2O_3 and YAG matrix. Analogously, some reported YAG-based glass-ceramics derived from controlled crystallization of multi component glasses, such as K_2O-SiO_2-Y_2O_3-Al_2O_3 [43], Y_2O_3-Al_2O_3-SiO_2 [44], and Li_2O-Y_2O_3-Al_2O_3-SiO_2 [45], have relatively low transparency on account of the light scattering caused by the refractive index difference between the YAG grains and glass matrix, but they exhibit practical photoluminescence properties. Considering the high theoretical YAG crystalline fraction (77 wt%), the YAG-Al_2O_3 nanoceramic drived from full crystalizatin of rare earth doped AY26 glass is predicted to have high photoluminescence efficiency. In particular, quantum efficiency as high as 87.5 % has been demonstrated in the YAG-based nanoceramics crystallized from AY26 glass at 1100 ℃ [22]. Thus, the YAG-Al_2O_3 nanoceramic is supposed to have promising applications in wide optical fields such as scintillators, laser diodes, and phosphor converters for high-power white-light LEDs. In the infrared region, the scattering effect decreases, so that the transparency of the resulting YAG-A_2O_3 nanoceramic is slightly higher than that of the stoichiometric YAG transparent ceramic, and is equivalent to that of YAG single crystal. The excellent infrared transmittance makes YAG-Al_2O_3 nanoceramic has potential infrared applications, such as infrared lamp, infrared thermal imaging system, infrared window and so on. It should be pointed out that the infrared cutoff wavelength (wavelength with a transmittance below 5%) of the transparent YAG-Al_2O_3 nanoceramic is about 6.5 μm, larger than that of YAG single crystal and YAG transparent ceramic (~6.1 μm). The larger infrared cutoff wavelength indicates that the transparent YAG-Al_2O_3 nanoceramic has lower phonon energy, which can effectively reduce the probability of electronic non-radiative transition and easier to obtain higher photoluminescence efficiency.

Hardness and Young's modulus of the YAG-Al_2O_3 nanoceramic crystallized at 963 ℃ for 2 h, YAG single crystal, and micrometer scale YAG transparent ceramic were measured using a nanoindenter. The indenter load and displacement were continuously recorded along with loading and unloading during the indentation process, as presented in Fig. 6(a). Under the same indentation depth, the load of the YAG-Al_2O_3 nanoceramic crystallized at 963 ℃ is almost the same as that of YAG single crystal and YAG transparent ceramic. The hardness and Young's modulus were determined from the data acquired during loading based on the Oliver-Pharr model [46]. As shown in Fig. 6(b), the YAG-Al_2O_3 nanoceramic crystallized at 963 ℃ show almost same hardness of 21 GPa with YAG single crystal and YAG transparent ceramic. The hardness of YAG-based nanoceramic crystallized at 1100 ℃ was reported as 23.6 GPa [22], higher than that of the nanoceramic obtained at 963 ℃. This may be because YAG and Al_2O_3 crystals are more fully developed at higher crystallization temperature, strengthening the three-dimensional network skeleton structure. Besides, the Young's modulus of the YAG-Al_2O_3 nanoceramic crystallized at 963 ℃ is 282 GPa, slightly lower than 297 GPa of YAG single crystal and YAG transparent ceramics. The hardness of YAG-Al_2O_3 nanoceramic crystallized at 963 ℃, comparable to that of YAG single crystal and YAG transparent ceramic, exhibits great potential for further applications.

4. Conclusions

The non-isothermal crystallization kinetics of the AY26 glass were investigated and highly transparent YAG-Al_2O_3 ceramics with fully dense nanostructure were elaborated by pressureless crystallization from the bulk AY26 glass at 963 ℃. The crystallization kinetics analyses show that the AY26 glass possesses high activation energy of more than 1500 kJ mol^{-1} resulting in excellent thermal stability. And its crystallization mechanism is the process of volume nucleation coupled with three-dimensional crystal growth. The resulting ceramics crystallized at 963 ℃ show similar nanostructures with the YAG-based nanoceramics crystallized at 1100 ℃, but consisting of obviously smaller YAG nanocrystals surrounded by homogeneous distributed thin Al_2O_3 areas. Consequently, the resulting YAG-Al_2O_3 nanoceramic crystallized at 963 □ has higher transmittance over the whole studied window than the YAG-based nanoceramic crystallized at 1100 ℃, and show higher infrared cutoff wavelength of 6.5 μm compared with YAG single crystal and YAG transparent ceramic (~6.1 μm). Besides, the YAG-Al_2O_3 nanoceramic crystallized at 963 ℃ show almost same hardness of 21 GPa with YAG single crystal and YAG transparent ceramic. Therefore, the combination of the crystallization kinetics analysis and glass crystallization technology could provide the theoretical guidance for the composition design of new kind of glass-crystallized nanoceramics, and drive the development of innovative optical ceramic materials in fields of laser diodes, scintillators, lenses, and high-power white-light LEDs.

Declaration of Competing Interest

The authors report no declarations of interest.

Acknowledgement

This work is financially supported by the National Key Research and Development Program of China (No. 2016YFC0700905), National Natural Science Foundation of China (NSFC No. 51972304, No. 51674232,

No. 51671181, No. 51971208), Beijing Municipal Science and Technology Project (No. Z191100004819002), The Project of Scientific Experiment on Chinese Manned Space Station, Chinese Academy of Sciences President's International Fellowship Initiative for 2021 (No. 2021VEA0012).

References

[1] A. Ikesue, L.A. Yan, Ceramic laser materials, Nat. Photonics 5 (2008) 721–727, https://doi.org/10.1038/nphoton.2008.243.

[2] G.L. Messing, A.J. Stevenson, Toward pore-free ceramics, Science 322 (2008) 383–384, https://doi.org/10.1126/science.1160903.

[3] T.R. Hinklin, S.C. Rand, R.M. Laine, Transparent, polycrystalline upconverting nanoceramics: towards 3-D displays, Adv. Mater. 20 (2008) 1270–1273, https://doi.org/10.1002/adma.200701235.

[4] R. Won, Ceramic future, Nat. Photonics 2 (2008) 340, https://doi.org/10.1038/nphoton.2008.104.

[5] H. Wang, Z. Huang, J. Qi, J. Wang, A new methodology to obtain the fracture toughness of YAG transparent ceramics, J. Adv. Ceram. 8 (2019) 418–426, https://doi.org/10.1007/s40145-019-0324-6.

[6] J. Ling, Y. Zhou, W. Xu, H. Lin, S. Lu, B. Wang, K. Wang, Red-emitting YAG:Ce,Mn transparent ceramics for warm WLEDs application, J. Adv. Ceram. 9 (2020) 45–54, https://doi.org/10.1007/s40145-019-0346-0.

[7] G. Zhang, D. Carloni, Y. Wu, Ultraviolet emission transparent Gd:YAG ceramics processed by solid-state reaction spark plasma sintering, J. Am. Chem. Soc. 103 (2020) 839–848, https://doi.org/10.1111/jace.16785.

[8] A. Wagner, B. Ratzker, S. Kalabukhov, S. Kolusheva, M. Sokol, N. Frage, Highly-doped Nd:YAG ceramics fabricated by conventional and high pressure SPS, Ceram. Int. 45 (2019) 12279–12284, https://doi.org/10.1016/j.ceramint.2019.03.141.

[9] A. Ikesue, I. Furusato, K. Kamata, Fabrication of polycrystalline, transparent YAG ceramics by a solid-state reaction method, J. Am. Chem. Soc. 78 (1995) 225–228, https://doi.org/10.1111/j.1151-2916.1995.tb08389.x.

[10] S.H. Lee, E.R. Kupp, A.J. Stevenson, J.M. Anderson, G.L. Messing, X. Li, E. C. Dickey, J.Q. Dumm, V.K. Simonaitis-Castillo, G.J. Quarles, Hot isostatic pressing of transparent Nd:YAG ceramics, J. Am. Chem. Soc. 92 (2009) 1456–1463, https://doi.org/10.1111/j.1551-2916.2009.03029.x.

[11] T. Irifune, K. Kawakami, T. Arimoto, H. Ohfuji, T. Kunimoto, T. Shinmei, Pressure-induced nano-crystallization of silicate garnets from glass, Nat. Commun. 7 (2016) 13753, https://doi.org/10.1038/ncomms13753.

[12] R. Zheng, J. Ding, Q. Zhang, B. Li, Z. Wang, C. Liu, P. Lv, K. Yu, W. Wei, Dy^{3+}-doped $Y_3Al_5O_{12}$ transparent ceramic for high efficiency ultraviolet excited single-phase white-emitting phosphor, J. Am. Chem. Soc. 102 (2019) 3510–3516, https://doi.org/10.1111/jace.16210.

[13] S. Alahraché, K. Al Saghir, S. Chenu, E. Véron, D.De S. Meneses, A.I. Becerro, M. Ocañ̃a, F. Moretti, G. Patton, C. Dujardin, F. Cussó, J.P. Guin, M. Nivard, J. C. Sangleboeuf, G. Matzen, M. Allix, Perfectly transparent $Sr_3Al_2O_6$ polycrystalline ceramic elaborated from glass crystallization, Chem. Mat. 25 (2013) 4017–4024, https://doi.org/10.1021/cm401953d.

[14] M. Allix, S. Alahrache, F. Fayon, M. Suchomel, F. Porcher, T. Cardinal, G. Matzen, Highly transparent $BaAl_4O_7$ polycrystalline ceramic obtained by full crystallization from glass, Adv. Mater. 24 (2012) 5570–5575, https://doi.org/10.1002/adma.201202282.

[15] M. Boyer, S. Alahraché, C. Genevois, M. Licheron, F.X. Lefevre, C. Castro, G. Bonnefont, G. Patton, F. Moretti, C. Dujardin, G. Matzen, M. Allix, Enhanced transparency through second phase crystallization in $BaAl_4O_7$ scintillating ceramics, Cryst. Growth Des. 16 (2016) 386–395, https://doi.org/10.1021/acs.cgd.5b01374.

[16] K. Al Saghir, S. Chenu, E. Veron, F. Fayon, M. Suchomel, C. Genevois, F. Porcher, G. Matzen, D. Massiot, M. Allix, Transparency through structural disorder a new concept for innovative transparent ceramics, Chem. Mater. 27 (2015) 508–514, https://doi.org/10.1021/cm5037106.

[17] A.J. Fernández-Carrión, K. Al Saghir, E. Veron, A.I. Becerro, F. Porcher, W. Wisniewski, G. Matzen, F. Fayon, M. Allix, Local disorder and tunable luminescence in $Sr_{1-x/2}Al_{2-x}Si_xO_4$ ($0.2 \leq x \leq 0.5$) transparent ceramics, Inorg. Chem. 56 (2017) 14446–14458, https://doi.org/10.1021/acs.inorgchem.7b01881.

[18] M. Boyer, A.J. Fernandez Carrion, S. Ory, A.I. Becerro, S. Villette, S.V. Eliseeva, S. Petoud, P. Aballea, G. Matzen, M. Allix, Transparent polycrystalline $SrREGa_3O_7$ melilite ceramics: potential phosphors for tuneable solid state lighting, J. Mater. Chem. C 4 (2016) 3238–3247, https://doi.org/10.1039/c6tc00633g.

[19] M. Boyer, X. Yang, A.J. Fernández Carrión, Q. Wang, E. Véron, C. Genevois, L. Hennet, G. Matzen, E. Suard, D. Thiaudière, C. Castro, D. Pelloquin, X. Kuang, M. Allix, First transparent oxide ion conducting ceramics synthesized by full crystallization from glass, J. Mater. Chem. A 6 (2018) 5276–5289, https://doi.org/10.1039/c7ta07621e.

[20] A. Bertrand, J. Carreaud, S. Chenu, M. Allix, E. Véron, J.-R. Duclère, Y. Launay, T. Hayakawa, C. Genevois, F. Brisset, F. Célarié, P. Thomas, G. Delaizir, Scalable and formable tellurite-based transparent ceramics for near infrared applications, Adv. Opt. Mater. 4 (2016) 1482–1486, https://doi.org/10.1002/adom.201600230.

[21] L. Mei, G. He, L.L. Wang, G.H. Liu, J.T. Li, Fabrication of transparent $LaAlO_3$/t-ZrO_2 nanoceramics through controlled amorphous crystallization, J. Eur. Ceram. Soc. 31 (2011) 1603–1609, https://doi.org/10.1016/j.jeurceramsoc.2011.03.004.

[22] X. Ma, X. Li, J. Li, C. Genevois, B. Ma, A. Etienne, C. Wan, E. Véron, Z. Peng, M. Allix, Pressureless glass crystallization of transparent yttrium aluminum garnet-based nanoceramics, Nat. Commun. 9 (2018) 1, https://doi.org/10.1038/s41467-018-03467-7.

[23] B.R. Johnson, W.M. Kriven, Crystallization kinetics of yttrium aluminum garnet ($Y_3Al_5O_{12}$), J. Mater. Res. 16 (2001) 1795–1805, https://doi.org/10.1557/JMR.2001.0248.

[24] G. He, L. Mei, L. Wang, G. Liu, J. Li, Synthesis and luminescence properties of nano-/microstructured $Y_3Al_5O_{12}:Ce^{3+}$ microspheres by controlled glass crystallization, Cryst. Growth Des. 11 (2011) 5355–5361, https://doi.org/10.1021/cg200939p.

[25] A. Prnová, A. Plško, J. Valúchová, K. Haladejová, R. Klement, D. Galusek, Crystallization kinetics of glass microspheres with yttrium aluminium garnet (YAG) composition, J. Therm. Anal. Calorim. 131 (2018) 1115–1123, https://doi.org/10.1007/s10973-017-6690-9.

[26] J. Chovanec, R. Svoboda, J. Kraxner, A. Cerna, D. Galusek, Crystallization kinetics of the $Y_3Al_5O_{12}$ glass, J. Alloys. Compd. 725 (2017) 792–799, https://doi.org/10.1016/j.jallcom.2017.07.191.

[27] D.W. Henderson, Thermal analysis of non-isothermal crystallization kinetics in glass forming liquids, J. Non-Cryst. Solids 30 (1979) 301–315, https://doi.org/10.1016/0022-3093(79)90169-8.

[28] T. Ozawa, Kinetics of non-isothermal crystallization, Polymer 12 (1971) 150–158, https://doi.org/10.1016/0032-3861(71)90041-3.

[29] K. Matusita, T. Komatsu, R. Yokota, Kinetics of non-isothermal crystallization process and activation energy for crystal growth in amorphous materials, J. Mater. Sci. 19 (1984) 291–296, https://doi.org/10.1007/BF00553020.

[30] W. Zhu, H. Jiang, H. Zhang, S. Jia, Y. Liu, Effect of TiO_2 and CaF_2 on the crystallization behavior of Y_2O_3-Al_2O_3-SiO_2 glass ceramics, Ceram. Int. 44 (2018) 6653–6658, https://doi.org/10.1016/j.ceramint.2018.01.076.

[31] Y. Bai, L. Peng, Q. Zhu, Z. Hao, Non-isothermal crystallization kinetics of stoichiometric lithium disilicate-based glasses with Al_2O_3 additives, J. Non-Cryst. Solids 445-446 (2016) 116–122, https://doi.org/10.1016/j.jnoncrysol.2016.05.032.

[32] G. Gupta, S. Balaji, K. Biswas, A. Kalyandurg, Mid-IR transparent TeO_2-TiO_2-La_2O_3 glass and its crystallization behavior for photonic applications, J. Am. Chem. Soc. 101 (2018) 3900–3916, https://doi.org/10.1111/jace.15558.

[33] P. Karmakar, A.K. Subudhi, K. Biswas, K. Annapurna, Crystallization kinetics analysis of BaF_2 and $BaGdF_5$ nanocrystals precipitated from oxyfluoride glass systems: a comparative study, Thermochim. Acta 610 (2015) 1–9, https://doi.org/10.1016/j.tca.2015.04.019.

[34] H.E. Kissinger, Variation of peak temperature with heating rate in differential thermal analysis, J Res. Natl. Bur. Stand. 57 (1956) 217–221, https://doi.org/10.6028/jres.057.026.

[35] J.A. Augis, J.E. Bennett, Calculation of the Avrami parameters for heterogeneous solid state reactions using a modification of the Kissinger method, J. Therm. Anal. 13 (1978) 283–292, https://doi.org/10.1007/BF01912301.

[36] T. Ozawa, A new method of analyzing thermogravimetric data, Bull. Chem. Soc. Jpn. 35 (1965) 1881–1886, https://doi.org/10.1246/bcsj.38.1881.

[37] K. Matusita, S. Sakka, Kinetic study of crystallization of glass by differential thermal analysis-criterion on application of Kissinger plot, J. Non-Cryst. Solids 38 (1980) 741–746, https://doi.org/10.1016/0022-3093(80)90525-6.

[38] K. Matusita, S. Sakka, Kinetic Study on non-isothermal crystallization of glass by thermal analysis, Bull. Inst. Chem. Res. KyotoUniv. 59 (1981) 159–171.

[39] A.L. Patterson, The Scherrer formula for X-ray particle size determination, Phys. Rev. 56 (1939) 978–982, https://doi.org/10.1103/PhysRev.56.978.

[40] C. Rüssel, Nanocrystallization of CaF_2 from $Na_2O/K_2O/CaO/CaF_2/Al_2O_3/SiO_2$ glasses, Chem. Mater. 17 (2005) 5843–5847, https://doi.org/10.1021/cm051430x.

[41] S. Bhattacharyya, C. Bocker, T. Heil, J.R. Jinschek, Thomas Höche, C. Rüssel, H. Kohl, Experimental evidence of self-limited growth of nanocrystals in glass, Nano Lett. 9 (2009) 2493–2496, https://doi.org/10.1021/nl901283r.

[42] D.E. Zelmon, D.L. Small, R. Page, Refractive-index measurements of undoped yttrium aluminum garnet from 0.4 to 5.0 μm, Appl. Opt. 37 (1998) 4933–4955, https://doi.org/10.1364/AO.37.004933.

[43] A. Tarafder, A.R. Molla, B. Karmakar, Processing and properties of Eu^{3+}-doped transparent YAG ($Y_3Al_5O_{12}$) nanoglass-ceramics, J. Am. Ceram. Soc. 93 (2010) 3244–3251, https://doi.org/10.1111/j.1551-2916.2010.03898.x.

[44] L.L. Wang, L. Mei, G. He, J.T. Li, L.H. Xu, Preparation of Ce:YAG glass-ceramics with low SiO_2, J. Am. Ceram. Soc. 1-4 (2011) 1–4, https://doi.org/10.1111/j.1551-2916.2011.04700.x.

[45] Y.H. Li, B.J. Chen, X. Zhao, Z.Q. Wang, H. Lin, Upconversion emissions in YAG glass ceramics doped with Tm^{3+}/Yb^{3+}